Numerical Exposure Assessment Report

SAR-NS_FCC-ISED-CE_6230346-A_DCB_V1.0

Customer: BURY GmbH & Co KG

Document Version 1.0 / 5th Dec, 2023

Author: David Schäfer

Numerical Exposure Assessment Report

Versions			
Release Date	**Nr.**	**Author**	**Comments**
5th December, 2023	1.0	David Schäfer	Initial version

Approval			
Name	**Job Title**	**Date**	**Signature**
David Schäfer	Preparation	5th Dec, 2023	
Jens Lerner	Review	5th Dec, 2023	

Laboratory	
Name and Address	IMST GmbH, Test Center Carl-Friedrich-Gauß-Str. 2–4 47475 Kamp-Lintfort
Accreditation	DAkkS Deutsche Akkreditierungsstelle D-PL-12139-01-01 The IMST GmbH is accredited by the German national "Deutsche Akkreditierungsstelle GmbH (DAkkS)" for testing according to the scope as listed in the accreditation certificate: D-PL-12139-01-02.

Customer (Applicant / Manufacturer[1])	
Name and Address	BURY GmbH & Co KG Robert-Koch-Str. 1-7 32584 Löhne, Germany Contact: Johann Dshus *Same as applicant*

Device Under Test (DUT)	
Type of DUT	Wireless power transfer charger with two charging slots
Model Name	DCB
FCC ID	QZ9-DCB
ISED Cert. No.	5927A-DCB
Frequency Band	128 kHz
Active Elements	Six coils (three per charging slot)

---

[1] If not the same as the applicant

Evaluation Results

Quantity inside flat phantom	Result*	Below exposure limit set by ...			
		ICNIRP	47 CFR § 1.1310	RSS-102	1999/ 519/EC
$SAR_{1g, max}$	83.4953 mW/kg	—**	Yes	Yes	—
$SAR_{10g, max}$	39.5694 mW/kg	Yes	Yes	Yes	Yes
$EIAV_{max}$	16.0917 V/m	Yes	—	Yes	—
*: Simulated values plus uncertainty penalties, cf. section 3.2.5					
**: Not applicable combinations were indicated as "—"					

Human Exposure Limits

Specific Absorption Rate (ICNIRP [1], 1999/519/EC [2])

Condition	Uncontrolled Environment (General Public)		Controlled Environment (Occupational)	
	SAR Limit	Mass Avg.	SAR Limit	Mass Avg.
SAR averaged over the whole body mass	0.08 W/kg	whole body	0.4 W/kg	whole body
Peak spatially-averaged SAR for the head, neck & trunk	2.0 W/kg	10 g of tissue*	10 W/kg	10 g of tissue*
Peak spatially-averaged SAR in the limbs/extremities	4.0 W/kg	10 g of tissue*	20 W/kg	10 g of tissue*
*: Defined as a tissue volume in the shape of a cube				

Specific Absorption Rate (RSS-102 [3, 4])

Condition	Uncontrolled Environment (General Public)		Controlled Environment (Occupational)	
	SAR Limit	Mass Avg.	SAR Limit	Mass Avg.
SAR averaged over the whole body mass	0.08 W/kg	whole body	0.4 W/kg	whole body
Peak spatially-averaged SAR for the head, neck & trunk	1.6 W/kg	1 g of tissue*	8 W/kg	1 g of tissue*
Peak spatially-averaged SAR in the limbs/extremities	4.0 W/kg	10 g of tissue*	20 W/kg	10 g of tissue*
*: Defined as a tissue volume in the shape of a cube				

Specific Absorption Rate (47 CFR Ch. I § 1.1310 [5])

Condition	Uncontrolled Environment (General Public)		Controlled Environment (Occupational)	
	SAR Limit	Mass Avg.	SAR Limit	Mass Avg.
SAR averaged over the whole body mass	0.08 W/kg	whole body	0.4 W/kg	whole body
Peak spatially-averaged SAR	1.6 W/kg	1 g of tissue*	8 W/kg	1 g of tissue*
Peak spatially-averaged SAR for extremities, such as hands, wrists, feet, ankles, and pinnae	4.0 W/kg	10 g of tissue*	20 W/kg	10 g of tissue*
*: Defined as a tissue volume in the shape of a cube				

Internal Electric Field (ICNIRP [1], RSS-102 [3, 4])

Condition	Uncontrolled Environment (General Public) EIAV Limit	Controlled Environment (Occupational) EIAV Limit
Peak EIAV @ f (in Hz)	$1.35 \cdot 10^{-4} \cdot f$ V/m	$2.7 \cdot 10^{-4} \cdot f$ V/m
Peak EIAV @ 128 kHz	17.28 V/m	34.56 V/m

Frequency Scopes

| Regulation | SAR | | EIAV |
	local	whole body	
ICNIRP	100 kHz — 6 GHz	100 kHz — 300 GHz	100 kHz — 10 MHz
47 CFR § 1.1310	100 kHz — 6 GHz		—*
RSS-102	100 kHz — 6 GHz		3 kHz — 10 MHz
1999/ 519/EC	100 kHz — 10 GHz		—
*: Not applicable combinations were indicated as "—"			

Contents

List of Figures

List of Tables

1 Introduction

1.1 Objective

The objective is the numerical exposure assessment of one Wireless Power Transfer (WPT) charger (further referred to as "device under test" or "DUT") designed by BURY GmbH & Co KG (further referred to as "customer"). In particular the Specific Absorption Rate (SAR, thermal hazard) and the internal electric field (EIAV[2], instantaneous nerve stimulation hazard) were investigated and compared to the exposure limits specified by ICNIRP [1], FCC [5], ISED [3, 4] and EUCO [2].

1.2 Simulation Method

All simulations were done with the Finite Difference Time Domain (FDTD) simulation tool Empire XPU [6]. A numerical model of the DUT was generated and validated by measurements of the magnetic field in its vicinity and measured inductance of the charging coils. The SAR and EIAV inside a flat phantom (human body part model) was investigated similar to the assessment procedures described in IEC/IEEE 62704-1 [7, 8]. The procedures were adapted to make them suitable for the low frequency of the DUT.

1.3 DUT Description

The 15 W, six coil wireless power charger "DCB" (further referred to as "device under test" or "DUT") can be used to simultaneously charge two portable devices like smart-phones (further referred to as "WPT receiver"). It is designed to be integrated into a vehicle, e.g. into the center console of a car. The DUT operates at a frequency of 128 kHz and features three charging coils per side, so six coils in total. During operation both sides can be excited/charging simultaneously, but only one of the three coils on each side is excited/charging at a time. Which coil is used for charging is chosen by the DUT itself, depending on the placement of the WPT receiver device. A photo of the DUT is depicted in Figure 1.

1.4 Setup for Reference Measurement

A validation of the numerical model was carried out by comparing the simulated magnetic field in the vicinity of the DUT with a reference measurement. The measurement was done on the behalf of the customer by the lab of "cetecom advanced GmbH" with the setup depicted in Figure 2. They used a "DASY8" positioner system from Speag and a "MAGPy-H3D" magnetic field probe with a $1\,cm^2$ "sensor size (loop)" and 6.6 mm "sensor center to tip distance". The measurements were done for a series production equivalent device, running in a testing operating mode at a fixed coil current of 3.5 A (RMS). The customer pre-determined this to be the maximum expectable coil current during charging a WPT receiver. No WPT receiver was present during the reference measurements of the magnetic field.

---

[2]EIAV is the particular name of the post-processing/visualisation feature in Empire XPU. The averaging is optional and was disabled for this investigation.

Figure 1: Photo of the DUT

Preliminary measurements showed that the worst-case configuration is given when both center coils from left and right charging slot are excited simultaneously, so only this operation state was considered. For the actual reference measurements the field probe was located directly above the xy-center of the left and right center coils, respectively. For each side a line measurement of the magnetic field strength was performed by lifting the probe upwards along the coil axis to different z-distances from the DUT. Figure 2 (a) shows the lowest possible position of the field probe (touch position) for the left side measurement.
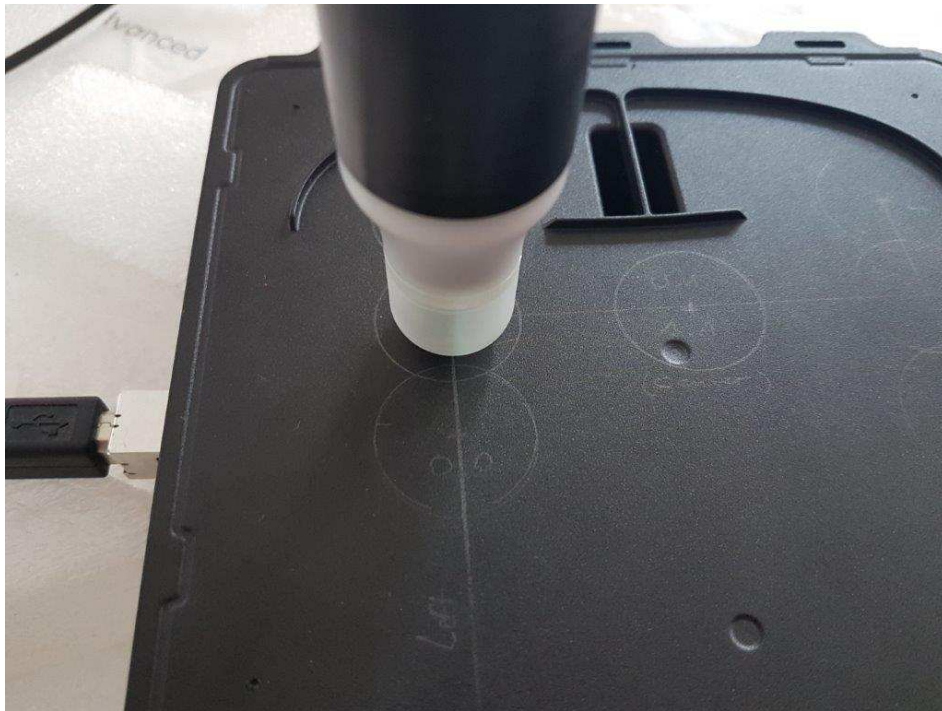
(a)

(b)

Figure 2: Measurement setup from the external lab of "cetecom advanced GmbH", showing (a) a close-up of the "MAGPy-H3D" probe in touch position on the left side and (b) the "DASY8" positioner (without DUT).

2 EM Simulation Model

2.1 Model Setup

The simulation model of the DUT is based on CAD data provided by the customer. The data was imported into Empire XPU and then rotated and moved so that the top of the DUTs housing is at $z = 0$ mm of the coordinate system. Figure 3 shows a top and bottom 3D view of the simulation model.

(a)   (b)

Figure 3: Geometry of the Empire simulation model of the DUT, showing the outer view on the top (a) and bottom (b) side.

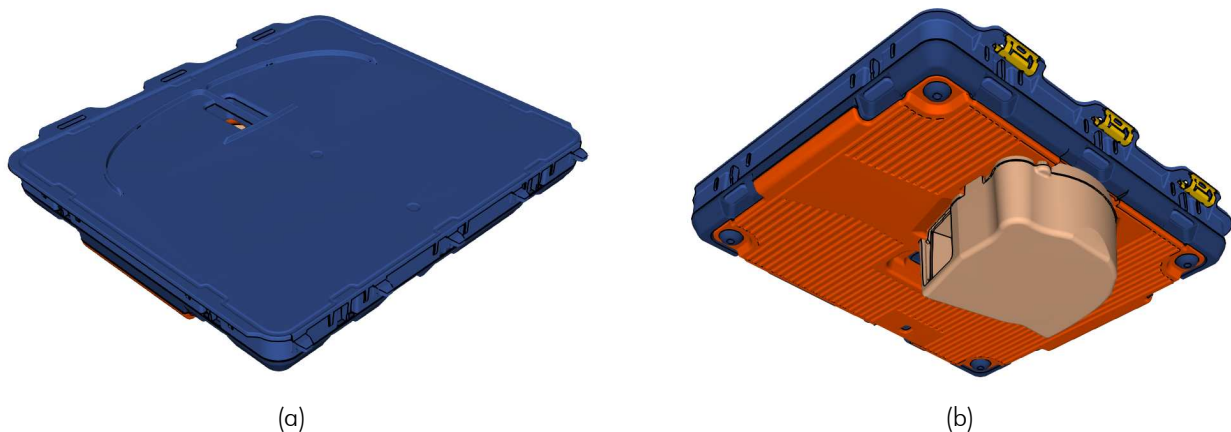In Figure 4 the internal components are visible, including the six WPT charging coils. The two center coils can be seen in yellow and blue, each located in the middle and overlapping the sideways coils. The middle points of the center coils are located at $x = -43.421$ mm (left), $x = +43.421$ mm (right), $y = 1.989$ mm (both), $z = -2.415$ mm (both) and the top side of the DUT housing is at $z = 0$ mm.

Figure 5 shows an exploded view of the most important components of the simulation model. Based on the customers information the material properties were set as follows:

(a) Housing top (PC+ABS, $\epsilon_r = 3.0$)
(b) Top PCB (Copper traces, $\sigma = 57.14857 \cdot 10^6$ S/m)
(c) WPT coils (Copper, $\sigma = 56.18 \cdot 10^6$ S/m)
(d) Ferrite plate ($\mu_r = 850$, $tan(\delta) = 0.0153$)
(e) Coil shield (AL6063 aluminum alloy, $\sigma = 30.3 \cdot 10^6$ S/m)
(f) Bottom PCB (Copper traces, $\sigma = 57.14857 \cdot 10^6$ S/m)
(g) Housing bottom (PC+ABS, $\epsilon_r = 3.0$)
(h) Heatsink (Aluminium, $\sigma = 38.0 \cdot 10^6$ S/m)
(i) Fan (Dielectric and PEC)
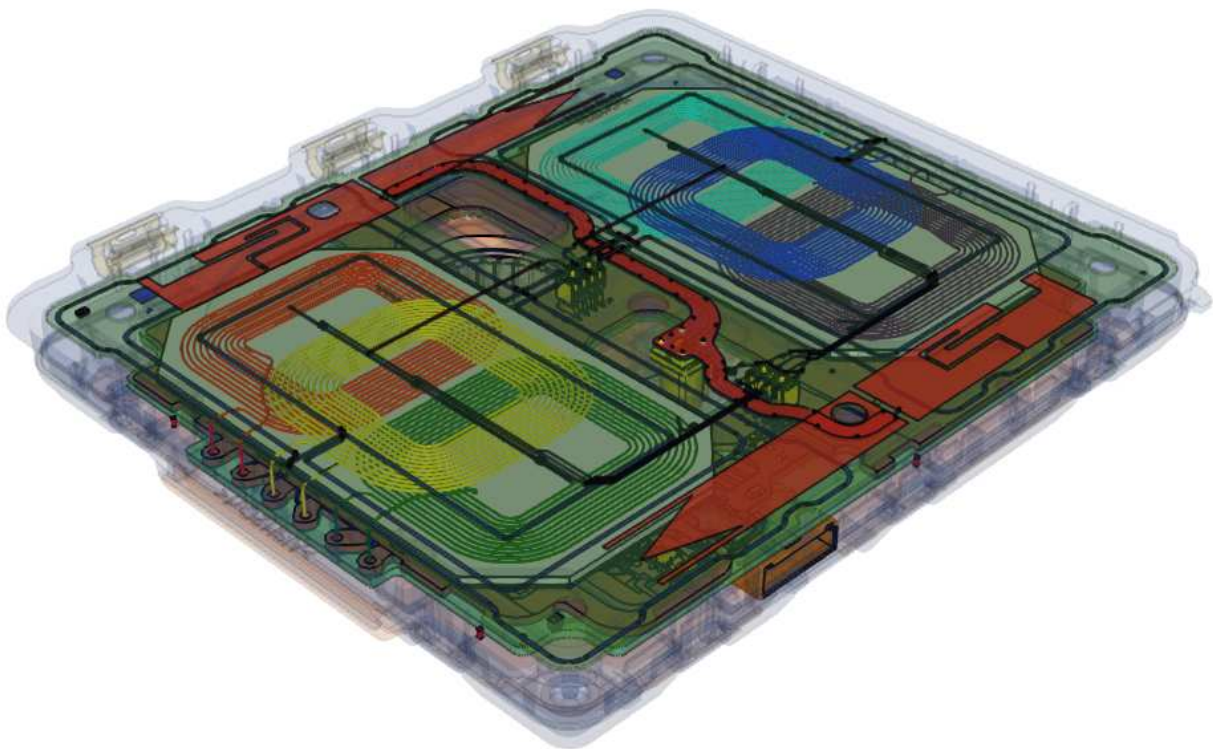
Figure 4: Geometry of the Empire simulation model of the DUT. The housing of the DUT is set transparent to show the internal components.
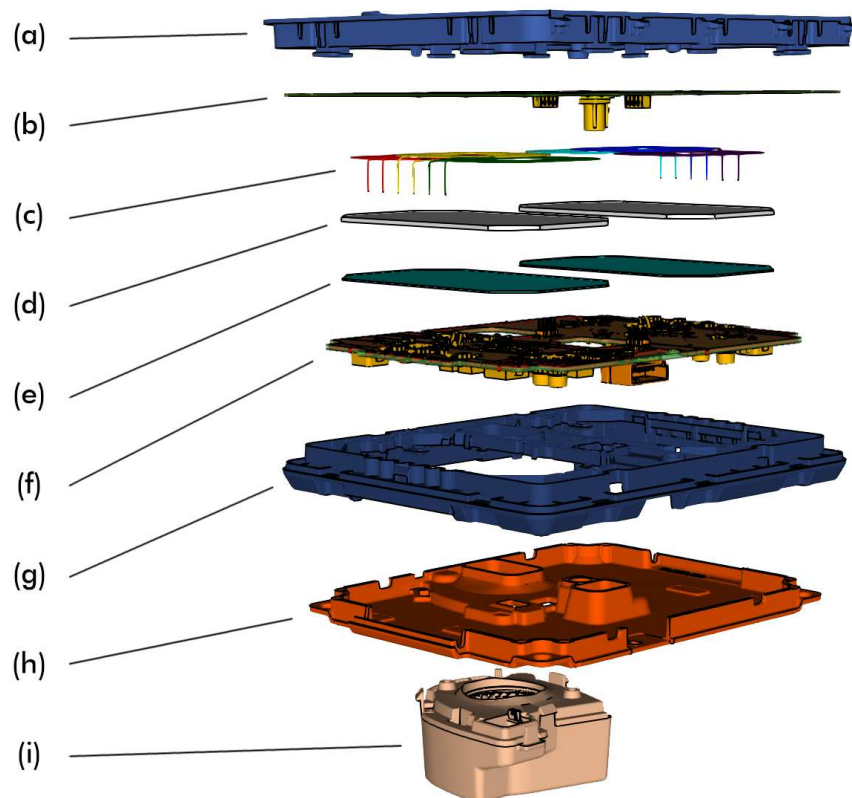
Figure 5: Geometry of the Empire simulation model of the DUT, showing an exploded view of the housing top (a), the top PCB (b), the WPT coils (c), the ferrite (d), the coil shield (e), the bottom PCB (f), the housing bottom (g), the heatsink (h) and the fan (i).

2.2   Model Check

The simulation model was checked by comparing the simulated magnetic fields with the reference measurement (cf. section 1.4). During measurement and simulation both central coils were excited with the maximum expectable current of $3.5\,A$ (RMS) at a frequency of $128\,kHz$. The sideways coils were inactive, so during the simulation their inputs were terminated with non-excited ports with $100\,k\Omega$ impedance. The simulation setup was unperturbed, meaning that it didn't include a WPT receiver device or phantom (human body model).

2.2.1   Magnetic Fields

Figure 6 shows a xz-cutplane for the simulated magnetic field strength through the center of the DUT. The colour legend is logarithmic with an 70 dB range. It can be seen how the main PCBs ground and the ferrite confine the main part of the magnetic field to the dedicated WPT receiver location above the DUT.
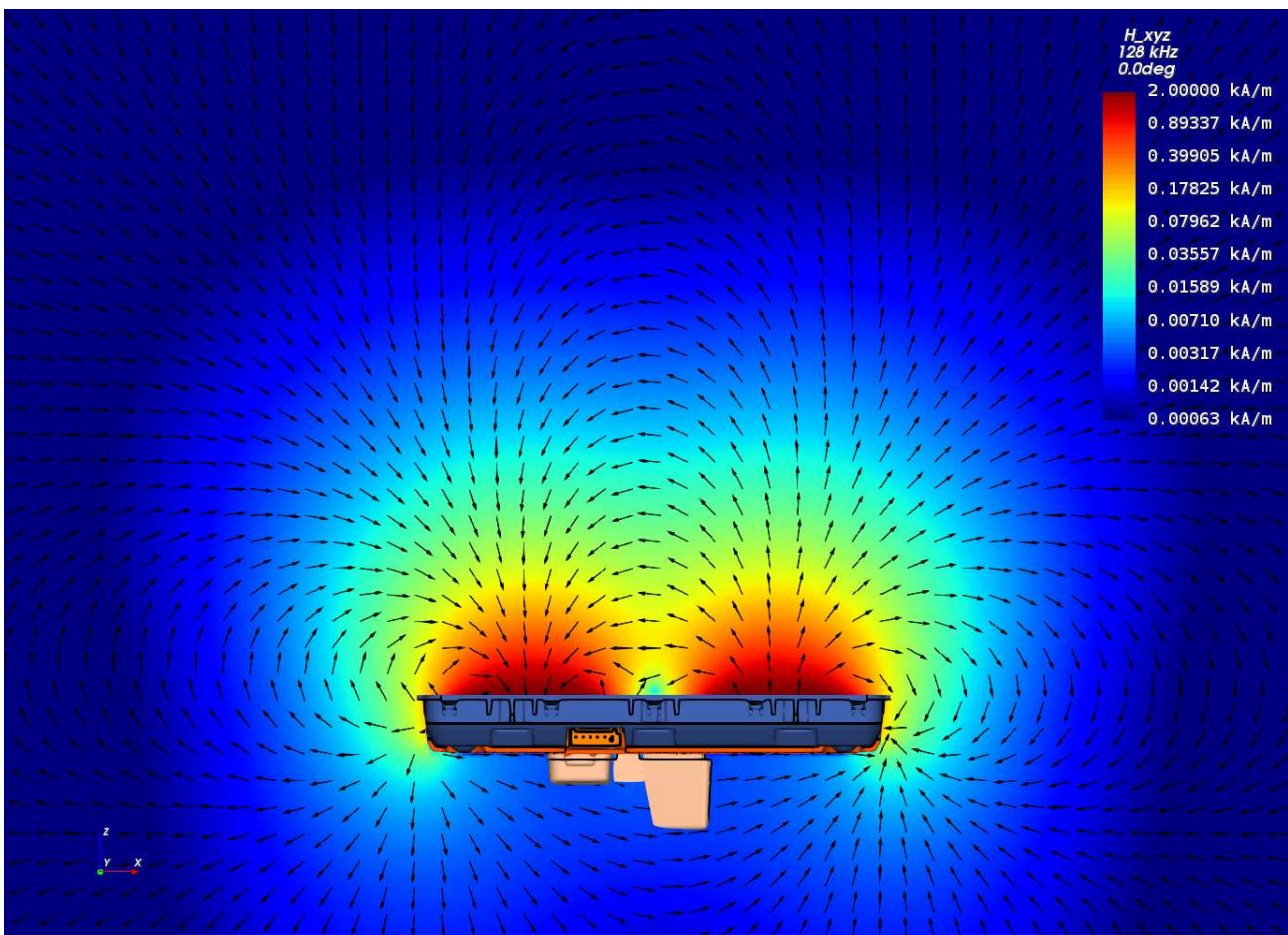
Figure 6: The simulated magnetic field displayed on a xz-plane through the DUT.

Analogue to the setup of the measurement (cf. section 1.4) the simulated magnetic field (H-field) strength was evaluated along the axis of the central coils for left and right side. The measurements start at $z = 6.6\,mm$ which corresponds to the "sensor center to tip distance" of the "MAGPy-H3D" field probe. The simulated lines start at $z = 0\,mm$ which is corresponds to the

top of the DUTs housing. As Figure 7 and Table 1 depict, the simulated H-field is in very good agreement with the measurements.

Coil Axis	Maximum Deviation
Left, Center	7.58 %
Right, Center	3.57 %

Table 1: Maximum deviation of simulated H-field lines from the corresponding measured H-field line for left and right side.

2.2.2   Coil Inductance

In addition to the magnetic fields also the inductance of the coil was used to check the simulation model. The measurement was done by the customer with the coil module taken out of the DUT. With a relative deviation of the center coils in each coil package of 6.93 % and 6.91 %, (cf. Table 2) the simulated inductance is in good agreement with the measurement.

Coil	Coil Inductance		Deviation
	Measured	Empire	
Left, Center	11.537 μH	12.337 μH	6.93 %
Right, Center	11.537 μH	12.335 μH	6.91 %

Table 2: Measured and simulated inductance.

2.2.3   Conclusion of Model Check

It can be concluded, that simulated magnetic field strength and inductance are in good agreement (cf. Figure 7 and Table 2) with the measurements from the external lab of "cetecom advanced GmbH", indicating the accurate setup of the Empire simulation model.

2.3   Phase Relation

The total superimposed field distribution and hence the exposure depends on the phase relation between the currents of the simultaneously operating left and right center coil. In-phase (0° phase shift) excitation as well as out-of-phase (180° phase shift) excitation were considered to determine and investigate the phase difference resulting in the highest exposure. However, it turned out that the highest 1g-SAR and 10g-SAR value occur for out-of-phase excitation while the highest EIAV value occurs for in-phase excitation. It was decided to use out-of-phase excitation for the numerical investigation and take into account the influence of the phase relation as an additional uncertainty component for the simulation parameter related uncertainty budget calculation (cf. Table 9 in section 3.2.1 below).
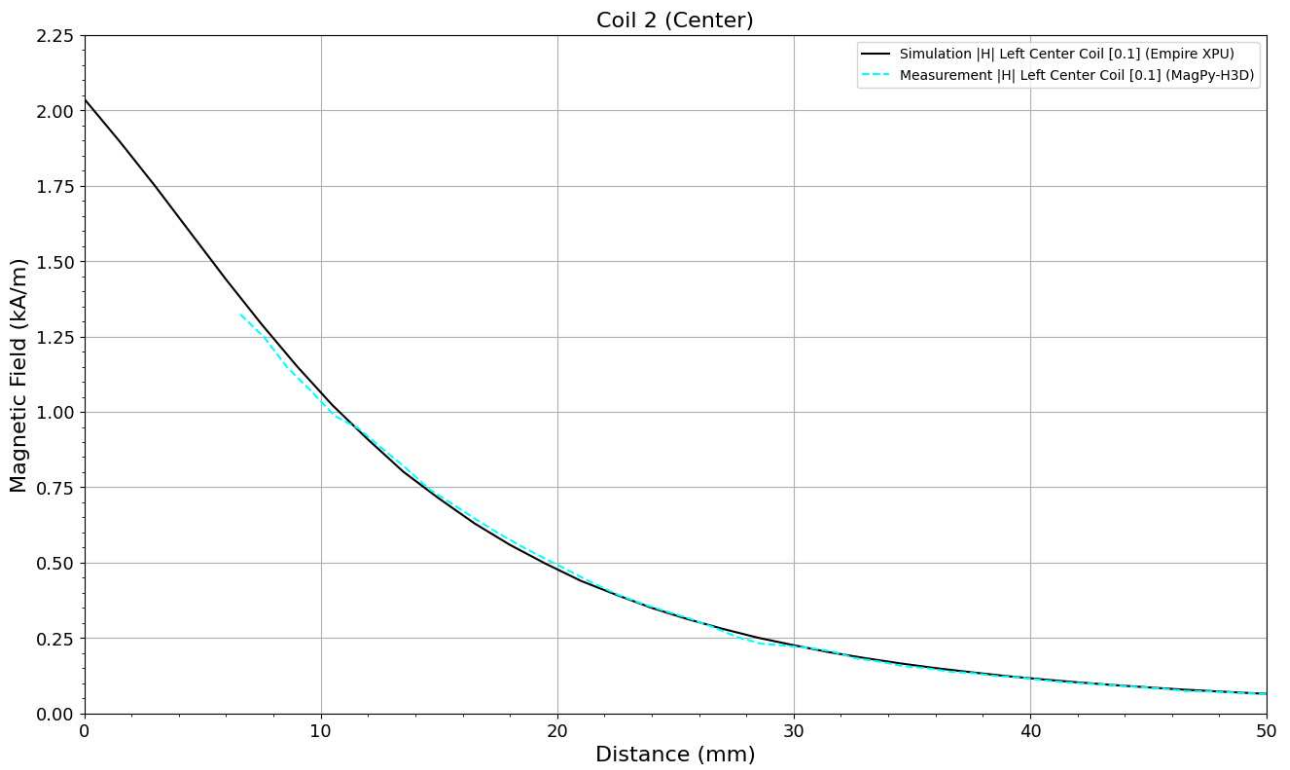
(a)
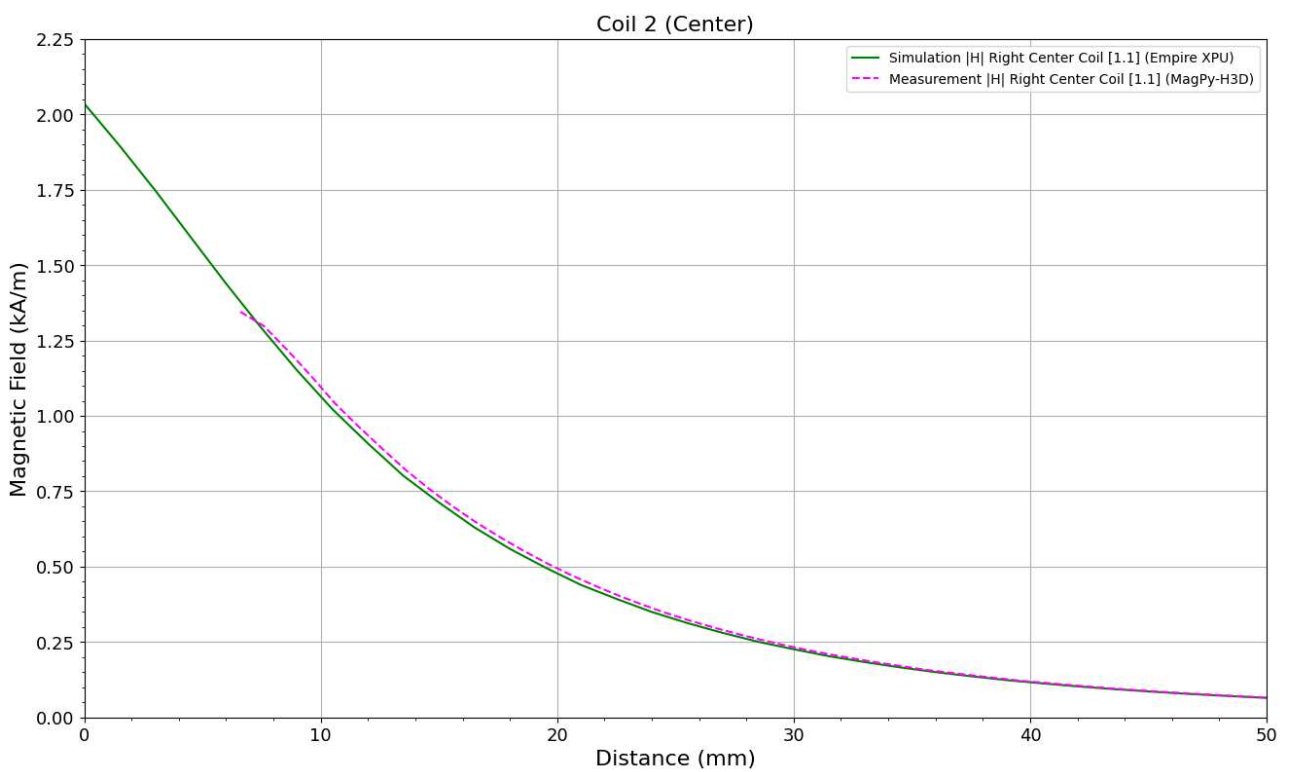
(b)

Figure 7: Curves for the line evaluation of the H-field (RMS values) for left (a) and right (b) side. The top of the DUT dielectric housing is located at $z = 0\,\mathrm{mm}$.

2.4   Air Grid

When the DUT is installed in a vehicle it is combined with an air grid (rubber mat), which is added on top of the DUTs housing as shown in Figure 8. The air grid allows air to pass by the bottom side of WPT receivers, cooling them during charging. Different variations of air grids can be combined with the DUT, depending on its mounting position inside the vehicle. The thinnest variant corresponding to the smallest possible separation distance was added to the numerical model and its material was set to TPS-SEBS ($\epsilon_r = 2.2$).

(a)

(b)

(c)

Figure 8: Geometry of the air grid (rubber mat) which was added on top of the DUT.

3　SAR and EIAV Evaluation

For the evaluation of the Specific Absorption Rate (SAR) and the internal Electric field (EIAV) a box shaped flat phantom was added to the simulation model. The setup resembles the situation of someone touching the DUT just after a receiver removal which was in "charging mode" at maximum field. For the SAR evaluation the coil currents could have been reduced according to the search mode duty cycle, but with respect to EIAV the continuous maximum expectable coil currents were retained throughout the investigation.

(a)　　　　　　　　　　　　　　　　　　　　　　(b)
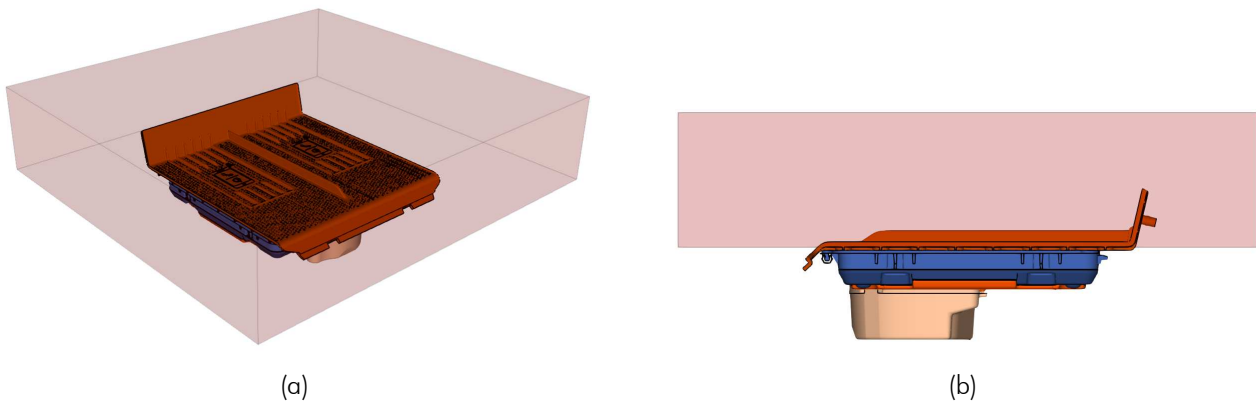
Figure 9: Geometry of the flat phantom in 3D view (a) and side view (b). The phantom was brought down to the lowest reachable parts of the air grid, i.e. the bottom of its crevices.

The phantom was centered (xy-direction) above the DUT at closest possible $z-$distance, virtually touching the lowest reachable parts of the air grid, i.e. the bottom of its crevices, as shown in Figure 9. With respect to the CAD coordinate system origin, the phantoms bottom side (side towards DUT) is located at $z = 1.7\,\mathrm{mm}$. The dimensions and the material properties of the phantom are as follows:

1. Geometric Size: $d_x \cdot d_y \cdot d_z = 335\,\mathrm{mm} \cdot 310\,\mathrm{mm} \cdot 72\,\mathrm{mm}$
2. Relative Permittivity: $\epsilon_r = 55$
3. Electrical Conductivity: $\sigma = 0.75\,\mathrm{S/m}$
4. Mass Density: $\rho = 1000\,\mathrm{kg/m^3} = 1\,\mathrm{g/cm^3}$

More details about the numerical model, like e.g. domain size, time step or total number of mesh cells, can be found in the appendix in section 4.1.

3.1　Simulation Results

Figure 10 shows the simulated 1g- and 10g-averaged SAR and Figure 11 shows the simulated un-averaged EIAV. Table 3 lists the corresponding maximum values and their positions.

3.2　Simulation Uncertainty

Based on chapter 7 of IEC/IEEE 62704-1 [7] the Combined- and Expanded Standard Uncertainty was calculated to analyse the accuracy of the results for the numerical model (further referred to
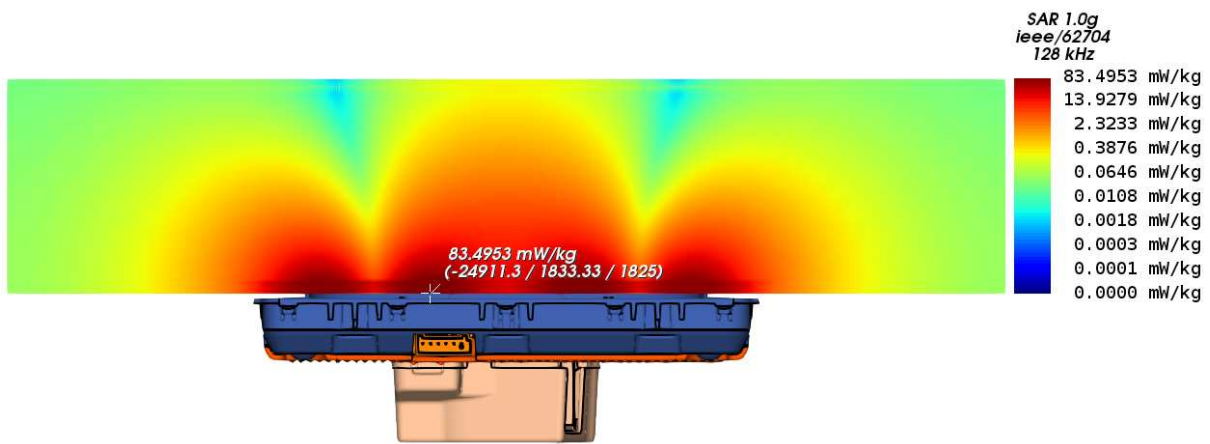
(a) Simulated 1g-averaged SAR
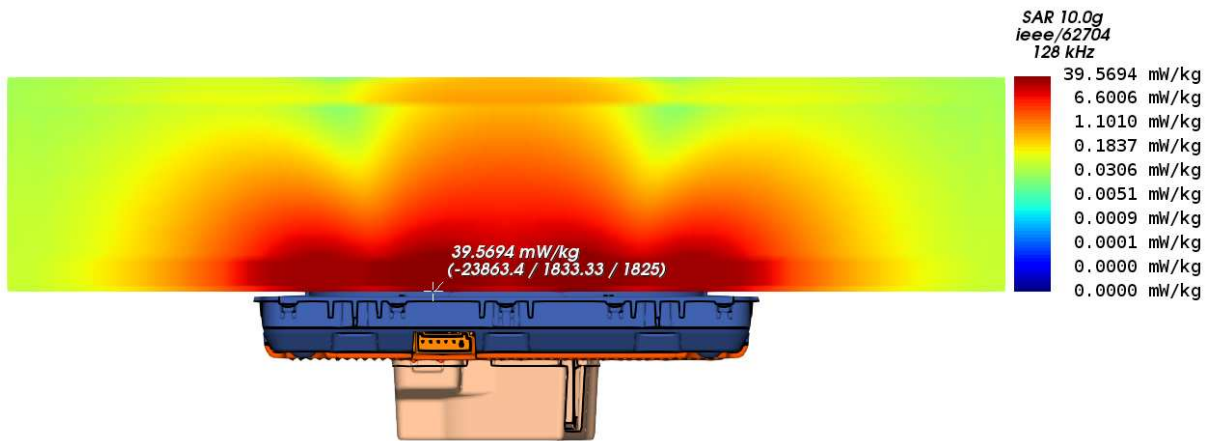
(b) Simulated 10g-averaged SAR

Figure 10: Cutplanes through the maxima of the simulated 1g-averaged SAR (a) and 10g-averaged SAR (b) inside the flat phantom. The phantom and air grid geometries are not visible. The discontinuities at the phantom boundaries are caused by the averaging algorithm (cf. [7, Section 6.2.2]).
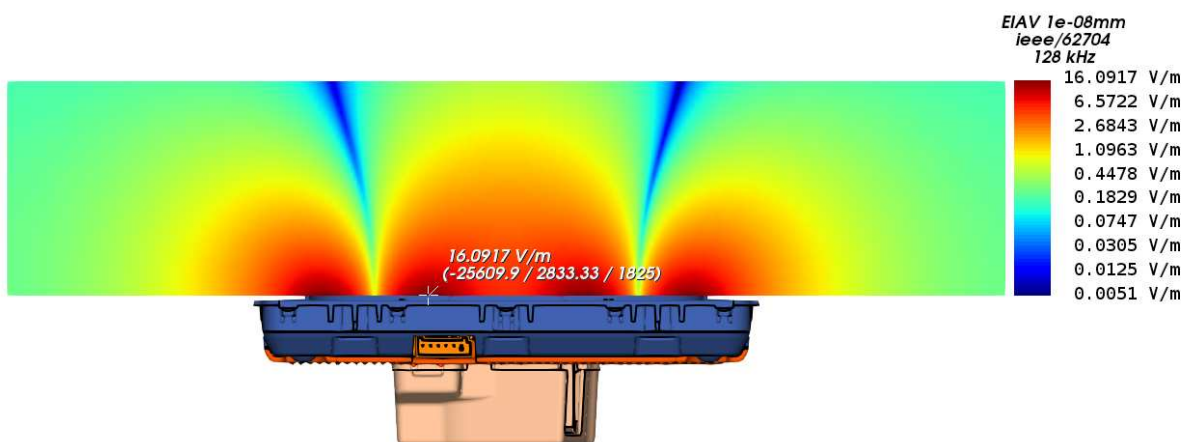
Figure 11: Cutplane through the maximum of the simulated EIAV inside the flat phantom. The phantom and air grid geometries are not visible.

Quantity	Maximum Value	Position of Maximum		
		x	y	z
$SAR_{1g,\,max}$	83.4953 mW/kg	−24.911 mm	1.833 mm	1.825 mm
$SAR_{10g,\,max}$	39.5694 mW/kg	−23.863 mm	1.833 mm	1.825 mm
$EIAV_{unaveraged,max}$	16.0917 V/m	−25.610 mm	2.833 mm	1.825 mm

Table 3: SAR and EIAV maximum values with their corresponding positions.

as "reported model"). Because the DUTs operating frequency is below the scope of the standard, the procedure had to be modified. Details about this will be described in the following sections.

3.2.1   Simulation Parameter Related Uncertainty

The procedure for evaluating the simulation parameter related uncertainty (IEC/IEEE 62704-1 [7, section 7.2]) was modified as described in Table 4. Table 5, 6, 7 and 8 show the maximum SAR and EIAV for the investigated variants as well as their relative deviation from the reported model. Table 10, 11 and 12 show the budget of the SAR and EIAV uncertainty contributions of the simulation parameters.

Uncertainty Component	Applicability of the Procedure from IEC/IEEE 62704-1 [7, section 7.2]	Number of Variations
Positioning	Applicable. Variation will be: Increase of distance between phantom and DUT by +1 mesh step	1
Mesh Resolution	Not 1:1 applicable. Requested refinement is not practicable at 128 kHz. Instead, total number of mesh cells will be increased by a factor of 2	1
Boundary Condition	Not 1:1 applicable, because $\lambda/4$ (=586 m) is way too large at 128 kHz. Instead, simulation domain will be enlarged by 50% simultaneously in +/- x/y/z direction	1
Power Budget	Not applicable. No travelling wave conditions are given, so comparison with power absorbed in ABC is not possible. Excitation will be normalized to fixed port/coil current.	0
Convergence	Not 1:1 applicable. Instead, variation will be simulated longer by a factor of 1.5 or more.	1
Phantom dielectrics	Not applicable / not indicated because fixed permittivity and conductivity from IEC/TR 62905 were used.	0
Phase Relation	Phase relations between left/right charging coil current. This uncertainty component is not contained in the standard. It was added for the reasons explained in section 2.3 and was considered with normal probability distribution (conservative, rectangular distribution may as well be justified).	1

Table 4: Description of the modified procedure for obtaining the simulation parameter related uncertainties.

Phantom z-Position	1.7 mm	1.95 mm
$SAR_{1g,\,max}$	83.4953 mW/kg	79.9751 mW/kg
$SAR_{10g,\,max}$	39.5694 mW/kg	38.0958 mW/kg
$EIAV_{max}$	16.0917 V/m	15.6904 V/m
$SAR_{1g,\,max}$-Deviation	0 %	−4.22 %
$SAR_{10g,\,max}$-Deviation	0 %	−3.72 %
EIAV-Deviation	0 %	−2.49 %

Table 5: SAR and EIAV results for different phantom positions. The first data column corresponds to the reported model (cf. section 3.1).

Mesh Resolution	20.3 MCells	41.9 MCells
$SAR_{1g,\,max}$	83.4953 mW/kg	85.3362 mW/kg
$SAR_{10g,\,max}$	39.5694 mW/kg	40.0978 mW/kg
$EIAV_{max}$	16.0917 V/m	16.4149 V/m
$SAR_{1g,\,max}$-Deviation	0 %	2.20 %
$SAR_{10g,\,max}$-Deviation	0 %	1.34 %
EIAV-Deviation	0 %	2.01 %

Table 6: SAR and EIAV results for different mesh resolutions. The first data column corresponds to the reported model (cf. section 3.1).

Domain Size	535 · 510 · 389.299 mm	1070 · 1020 · 778.598 mm
$SAR_{1g,\,max}$	83.4953 mW/kg	83.4380 mW/kg
$SAR_{10g,\,max}$	39.5694 mW/kg	39.5334 mW/kg
$EIAV_{max}$	16.0917 V/m	16.0852 V/m
$SAR_{1g,\,max}$-Deviation	0 %	−0.07 %
$SAR_{10g,\,max}$-Deviation	0 %	−0.09 %
EIAV-Deviation	0 %	−0.04 %

Table 7: SAR and EIAV results for different simulation domain sizes. The first data column corresponds to the reported model (cf. section 3.1). The simulation domain was enlarged symmetrically in all spatial directions.

Time/Convergence	11 Msteps	17 Msteps
Energy Decay	$-102.2\,\mathrm{dB}$	$-103.5\,\mathrm{dB}$
$SAR_{1g,\,max}$	$83.4953\,\mathrm{mW/kg}$	$83.5247\,\mathrm{mW/kg}$
$SAR_{10g,\,max}$	$39.5694\,\mathrm{mW/kg}$	$39.5864\,\mathrm{mW/kg}$
$EIAV_{max}$	$16.0917\,\mathrm{V/m}$	$16.0944\,\mathrm{V/m}$
$SAR_{1g,\,max}$-Deviation	$0\,\%$	$0.04\,\%$
$SAR_{10g,\,max}$-Deviation	$0\,\%$	$0.04\,\%$
EIAV-Deviation	$0\,\%$	$0.02\,\%$

Table 8: SAR and EIAV results for different number of total time steps. The first data column corresponds to the reported model (cf. section 3.1).

Phase Relation	Out-of-Phase	In-Phase
$SAR_{1g,\,max}$	$83.4953\,\mathrm{mW/kg}$	$82.5467\,\mathrm{mW/kg}$
$SAR_{10g,\,max}$	$39.5694\,\mathrm{mW/kg}$	$38.6655\,\mathrm{mW/kg}$
$EIAV_{max}$	$16.0917\,\mathrm{V/m}$	$16.1253\,\mathrm{V/m}$
$SAR_{1g,\,max}$-Deviation	$0\,\%$	$-1.14\,\%$
$SAR_{10g,\,max}$-Deviation	$0\,\%$	$-2.28\,\%$
EIAV-Deviation	$0\,\%$	$0.21\,\%$

Table 9: SAR and EIAV results for different phase relations between coil currents of left/right center coils. The first data column corresponds to the reported model (cf. section 3.1).

Uncertainty Component	Section in [7]	1g-SAR Tolerance in %	Probability Distribution	Divisor	c_i	1g-SAR Uncertainty in %
Positioning	7.2.1	$-4.22\,\%$	R	1.73	1	$-2.44\,\%$
Mesh Resolution	7.2.2	$2.20\,\%$	N	1	1	$2.20\,\%$
Boundary Condition	7.2.3	$-0.07\,\%$	N	1	1	$-0.07\,\%$
Power Budget	7.2.4	*not appl.*	N	1	1	*not appl.*
Convergence	7.2.5	$0.04\,\%$	R	1.73	1	$0.02\,\%$
Phantom dielectrics	7.2.6	*not appl.*	R	1.73	1	*not appl.*
Phase Relation	-	$-1.14\,\%$	N	1	1	$-1.14\,\%$
Combined Std. Uncertainty (k=1)						$3.48\,\%$

Table 10: Budget of the 1g-SAR uncertainty contributions of the simulation parameters, corresponding to IEC/IEEE 62704-1 [7, Table 3]. Note: N, R, U = normal, rectangular, U-shaped probability distributions.

Uncertainty Component	Section in [7]	10g-SAR Tolerance in %	Probability Distribution	Divisor	c_i	10g-SAR Uncertainty in %
Positioning	7.2.1	-3.72%	R	1.73	1	-2.15%
Mesh Resolution	7.2.2	1.34%	N	1	1	1.34%
Boundary Condition	7.2.3	-0.09%	N	1	1	-0.09%
Power Budget	7.2.4	*not appl.*	N	1	1	*not appl.*
Convergence	7.2.5	0.04%	R	1.73	1	0.02%
Phantom dielectrics	7.2.6	*not appl.*	R	1.73	1	*not appl.*
Phase Relation	-	-2.28%	N	1	1	-2.28%
Combined Std. Uncertainty (k=1)						3.41%

Table 11: Budget of the 10g-SAR uncertainty contributions of the simulation parameters, corresponding to IEC/IEEE 62704-1 [7, Table 3]. Note: N, R, U = normal, rectangular, U-shaped probability distributions.

Uncertainty Component	Section in [7]	EIAV Tolerance in %	Probability Distribution	Divisor	c_i	EIAV Uncertainty in %
Positioning	7.2.1	-2.49%	R	1.73	1	-1.44%
Mesh Resolution	7.2.2	2.01%	N	1	1	2.01%
Boundary Condition	7.2.3	-0.04%	N	1	1	-0.04%
Power Budget	7.2.4	*not appl.*	N	1	1	*not appl.*
Convergence	7.2.5	0.02%	R	1.73	1	0.01%
Phantom dielectrics	7.2.6	*not appl.*	R	1.73	1	*not appl.*
Phase Relation	-	0.21%	N	1	1	0.21%
Combined Std. Uncertainty (k=1)						2.48%

Table 12: Budget of the EIAV uncertainty contributions of the simulation parameters, analogue to the budget of the SAR uncertainty contributions of the simulation parameters to IEC/IEEE 62704-1 [7, Table 3]. Note: N, R, U = normal, rectangular, U-shaped probability distributions.

3.2.2 Model Related Uncertainty

For distances $d < \lambda/2$ the IEC/IEEE 62704-1 [7, section 7.3.3] states that "*[...] the only way to determine the uncertainty of the DUT model is by SAR measurements*", which is not possible for the given frequency of the DUT. Therefore the procedure was modified by using the squared H-field values instead of SAR in [7, equation 14], similar to the assessment for distances $d \geq \lambda/2$ by [7, equation 13]. The H-field lines from both charging slots were considered, whereby the maximum value occurred for the left side.

$$U_{\mathrm{sim,model}} = max \left(\frac{|H^2_{\mathrm{ref,n}} - H^2_{\mathrm{sim,n}}|}{H^2_{\mathrm{ref,max}}} \right) \tag{1}$$

$$= \left[\frac{|(1323.57\,\mathrm{A/m})^2 - (1379.62\,\mathrm{A/m})^2|}{(1323.57\,\mathrm{A/m})^2} \right]_{\substack{z=6.60\,\mathrm{mm} \\ x=-43.42\,\mathrm{mm}}} \tag{2}$$

$$= 8.65\,\% \tag{3}$$

Table 13 shows the budget of the uncertainty contributions of the model parameter. The customer stated an k=2 uncertainty of $1.24\,\mathrm{dB} \Rightarrow 7.67\,\%$ for the measurements done by "cetecom advanced GmbH" (cf. section 1.4), so $7.67\,\%$ was used for the k=1 uncertainty of the measurement equipment and procedure.

Uncertainty Component (SAR)	Section in [7]	Tolerance in %	Probability Distribution	Divisor	c_i	Uncertainty in %
Uncertainty of the DUT model	7.3.2 or 7.3.3	8.65 %	N	1	1	8.65 %
Uncertainty of the phantom model	7.3.3	*not appl.*	N	1	1	*not appl.*
Uncertainty of the measurement equipment and procedure	-	7.67 %	N	1	1	7.67 %
Combined Std. Uncertainty (k=1)						9.16 %

Table 13: Budget of the uncertainty contributions of the model setup, corresponding to IEC/IEEE 62704-1 [7, Table 4]. Note: N, R, U = normal, rectangular, U-shaped probability distributions.

3.2.3 Model Validation

To validate the numerical model the equation 15 from IEC/IEEE 62704-1 [7, section 7.3.4] was calculated for the H-field line evaluation. The H-field lines from both charging slots were considered, whereby the maximum value occurred for the left side.

$$E_n = max \left(\sqrt{\frac{(\nu_{\text{sim,n}} - \nu_{\text{ref,n}})^2}{(\nu_{\text{sim,n}} U_{\text{sim(k=2)}})^2 + (\nu_{\text{ref,n}} U_{\text{ref(k=2)}})^2}} \right) \tag{4}$$

$$= max \left(\sqrt{\frac{(H_{\text{sim,n}}^2 - H_{\text{ref,n}}^2)^2}{(H_{\text{sim,n}}^2 U_{\text{sim(k=2)}})^2 + (H_{\text{ref,n}}^2 U_{\text{ref(k=2)}})^2}} \right) \tag{5}$$

$$= \left[\sqrt{\frac{((249.19\,\text{A/m})^2 - (231.64\,\text{A/m})^2)^2}{((249.19\,\text{A/m})^2 \cdot (17.30\,\%))^2 + ((231.64\,\text{A/m})^2 \cdot (15.35\,\%))^2}} \right]_{\substack{z=28.60\,\text{mm} \\ x=-43.42\,\text{mm}}} \tag{6}$$

$$= 0.62 \leq 1 \tag{7}$$

The condition/inequation is fulfilled, indicating that the deviation is within the expected uncertainty, and hence that the model is valid.

3.2.4   Uncertainty Budget

The budgets for simulation parameters related uncertainties and model related uncertainties were combined (k=1) and expanded (k=2) for 1g-SAR, 10g-SAR and EIAV as shown in table 14, 15 and 16.

3.2.5   Uncertainty Penalty

The calculated Expanded Std. Uncertainties for SAR/EIAV do not exceed the maximum of 30 % stated in IEC/IEEE 62704-1 [7, Section 7.4]. Therefore uncertainty penalties as described in EN 62311 [9, Section 6.2, Equation 1] were not applied.

Uncertainty Component (1g-SAR)	Section in [7]	Tolerance in %	Probability Distribution	Divisor	c_i	Uncertainty in %
Uncertainty of the DUT model with respect to simulation parameters	7.2	3.48 %	N	1	1	3.48 %
Uncertainty of the developed numerical model of the DUT	7.3	9.16 %	N	1	1	9.16 %
Combined Std. Uncertainty (k=1)						9.38 %
Expanded Std. Uncertainty (k=2)						18.75 %

Table 14: Combined and expanded budget of the 1g-SAR uncertainty, corresponding to IEC/IEEE 62704-1 [7, Table 5]. Note: N, R, U = normal, rectangular, U-shaped probability distributions.

Uncertainty Component (10g-SAR)	Section in [7]	Tolerance in %	Probability Distribution	Divisor	c_i	Uncertainty in %
Uncertainty of the DUT model with respect to simulation parameters	7.2	3.41 %	N	1	1	3.41 %
Uncertainty of the developed numerical model of the DUT	7.3	9.16 %	N	1	1	9.16 %
Combined Std. Uncertainty (k=1)						9.37 %
Expanded Std. Uncertainty (k=2)						18.73 %

Table 15: Combined and expanded budget of the 10g-SAR uncertainty, corresponding to IEC/IEEE 62704-1 [7, Table 5]. Note: N, R, U = normal, rectangular, U-shaped probability distributions.

| Uncertainty Component (EIAV)	Section in [7]	Tolerance in %	Probability Distribution	Divisor	c_i	Uncertainty in %
Uncertainty of the DUT model with respect to simulation parameters	7.2	2.48 %	N	1	1	2.48 %
Uncertainty of the developed numerical model of the DUT	7.3	9.16 %	N	1	1	9.16 %
Combined Std. Uncertainty (k=1)						9.27 %
Expanded Std. Uncertainty (k=2)						18.54 %

Table 16: Combined and expanded budget of the EIAV uncertainty, analogue to the budget of the SAR uncertainty from IEC/IEEE 62704-1 [7, Table 5]. Note: N, R, U = normal, rectangular, U-shaped probability distributions.
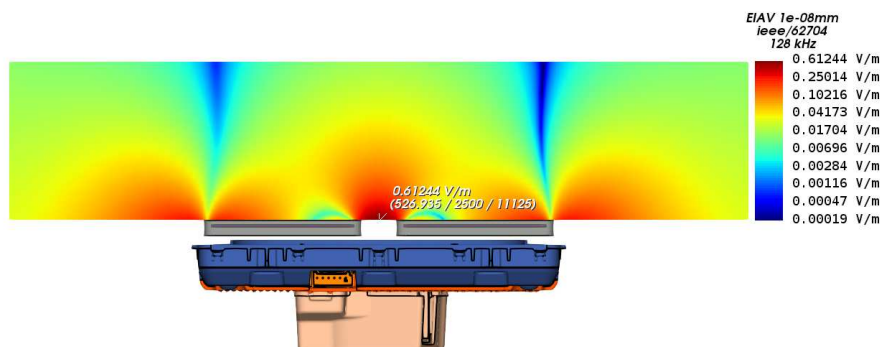
3.3   Passive Receiver Impact

In the reported model the phantom is directly placed onto the DUT. However, usually a WPT receiver such as a handset is placed on top of the DUT during charging operation. A receiver would increase the smallest possible approach distance, and its metal parts would act as a shield for the E- and H-fields, hence decreasing the exposure. To illustrate this effect, an additional simulation was done, whereby two passive phone receiver dummies were added to the model (cf. Figure 12). Table 17 lists the maximum values for 1g-SAR, 10g-SAR and EIAV and their positions for model with the passive receiver dummies. As expected they are noticeable lower than in case of the reported model. The before mentioned shielding effect also qualitatively changes the SAR/EIAV distribution, as can be seen in Figure 13.

Quantity	Reported Model	With Passive Receiver
$SAR_{1g, max}$	83.4953 mW/kg	0.09947 mW/kg
$SAR_{10g, max}$	39.5694 mW/kg	0.03764 mW/kg
$EIAV_{unaveraged,max}$	16.0917 V/m	0.61244 V/m

Table 17: SAR and EIAV maximum values for the model with the passive receiver dummy.

(a)   (b)
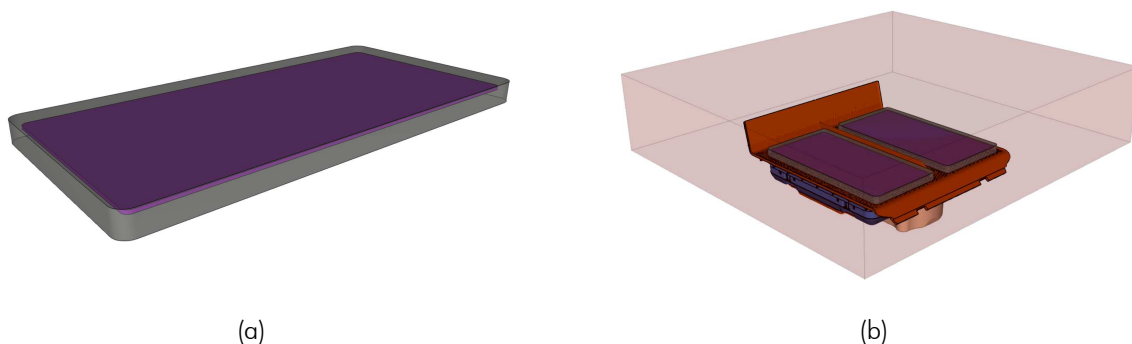
Figure 12: Geometry of the passive receiver dummy, consisting of a $145 \cdot 70 \cdot 7$ mm dielectric housing with a metal plate inside (a). The receiver dummy was placed in between DUT and phantom (b).

Figure 13: Cutplane through the maximum of the simulated EIAV inside the flat phantom for the model with the passive receiver dummies. The air grid is invisible in this plot but was contained in the simulation.

3.4 Conclusion of the Evaluation

Summarizing the numerical exposure assessment of the DUT, the following can be stated:

1. The simulated magnetic field strength and the coil inductance are in good agreement with the measurements (cf. section 2.2), indicating the accurate setup of the DUT simulation model (without phantom).

2. The investigated scenario (reported model) follows the worst-case assumption that:

   (a) The flat phantom is in direct contact with the DUT with no receiver in between.

   (b) The DUT is exciting its two center coils simultaneously with the maximum expectable current, despite the fact that no receiver device is present.

   (c) The search mode duty cycle is neglected.

3. The model validation (cf. section 3.2.3) shows that in-equation 15 from IEC/IEEE 62704-1 is fulfilled, indicating a valid numerical model.

4. The uncertainty analysis returns Expanded Standard Uncertainties below the permissible 30% stated in IEC/IEEE 62704-1 section 7.4.

5. The evaluated maximum 1g-averaged SAR is $83.4953\,\text{mW/kg}$.

6. The evaluated maximum 10g-averaged SAR is $39.5694\,\text{mW/kg}$.

7. The evaluated maximum EIAV (internal Electric field, nerve stimulation hazard) is $16.0917\,\text{V/m}$.

8. The following interpretation of the assessment results (decision rule) is carried out on the basis of ILAC-G8:09/2019, chap. 4.2.1 according to the "Simple Acceptance" decision rule - as far as this is not contradicted by other normative requirements.

9. With respect to the statements above, the conclusion of this numerical exposure assessment report is, that the DUT does not exceed the SAR and/or EIAV exposure limits specified by ICNIRP [1], FCC [5], ISED [3, 4] and EUCO [2]. A tabular evaluation can be found at the beginning of the report.

4 Appendix

4.1 Specific Information for Computational Modelling

Computational resources Computation was performed on a dual Intel Xeon 2697v3 14-core processor with 11.435 GB memory usage.

FDTD algorithm implementation and validation cf. [8]

Computing peak SAR from field components cf. [8]

1g-averaged SAR procedures cf. [7, 8]

Computational parameters for reported model:

 Cell Size (min/max): 0.25 mm / 10.37 mm

 Domain Size: $535 \cdot 510 \cdot 389.299$ mm

 Total amount of mesh cells: approx. 20.3 million

 Time step: $2.40279 \cdot 10^{-13}$ s

 Total number of time steps: approx. 11 million

 Simulation time: approx. 13 hours and 57 minutes

 Simulation speed: 4508.742 million cells per second (4.508 GCells/s).

 Excitation method: Gaussian pulse with $f_0 = 0$ Hz, $f_{BW} = 50$ MHz

Phantom model implementation cf. section 3

Tissue dielectric parameters cf. section 3

Transmitter model implementation and validation cf. section 2

Test device positioning cf. section 3

Steady state termination procedures A Gaussian pulse was used for the excitation and the simulation was terminated when the energy has dissipated to more than -102 dB.

Test results cf. section 3

4.2   Abbreviations

Abbreviation	Description
CAD	Computer Aided Design
DUT	Device Under Test
EIAV	Averaged Internal Electric Field
EM	Electro Magnetic
FDTD	Finite Difference Time Domain
PCB	Printed Circuit Board
RF	Radio Frequency
RMS	Root Mean Square
SAR	Specific Absorption Rate
S/m	Siemens per meter $= 1/(\Omega m)$

Table 18: Abbreviations.

4.3   Remarks

This report relates only to the item(s) evaluated. This report shall not be reproduced, except in its entirety, without the prior written approval of IMST GmbH. The results and statements contained in this report reflect the evaluation for the certain model described above. The manufacturer is responsible for ensuring that all production devices meet the intent of the requirements described in this report.

5   References

[1] International Commission on Non-Ionizing Radiation Protection (ICNIRP), "ICNIRP Guidelines for limitting Exposure to Electromagnetic Fields (100 KHz to 300 GHz)," 2020.

[2] European Council, "Council Recommendation of 12 July 1999 on the limitation of exposure of the general public to electromagnetic fields (0 Hz to 300 GHz), 1999/519/EC," July 1999.

[3] Innovation, Science and Economic Development Canada (ISED, Canada), "RSS-102 Issue 5 - Radio Frequency (RF) Exposure Compliance of Radiocommunication Apparatus (All Frequency Bands), with Amendment 1 from February 2, 2021," March 2015.

[4] ——, "SPR-002 Issue 2 - Supplementary Procedure for Assessing Compliance of Equipment Operating from 3 kHz to 10 MHz with RSS-102," October 2022.

[5] Federal Communications Commission (FCC, USA), "FCC Limits for Specific Absorption Rate (SAR), 47 C.F.R. § 2.1093, 10-1-20 Edition," 2020.

[6] IMST GmbH. (2023, September) Empire XPU, Version 8.2. Carl-Friedrich-Gauß-Str. 2-4, 47475 Kamp-Lintfort, Germany. [Online]. Available: http://empire.de

[7] "IEC/IEEE International Standard – Determining the peak spatial-average specific absorption rate (SAR) in the human body from wireless communications devices, 30 MHz to 6 GHz - Part 1: General requirements for using the finite-difference time-domain (FDTD) method for SAR calculations," *IEC/IEEE 62704-1:2017*, pp. 1–86, 2017.

[8] IMST GmbH, "Empire XPU - Code Verification Report for IEC/IEEE 62704-1, Version 8.2," February 2023.

[9] CENELEC, "Assessment of electronic and electrical equipment related to human exposure restrictions for electromagnetic fields (0 Hz to 300 GHz), EN IEC 62311," January 2020.